Intrusion Detection based on k-coverage in Mobile Sensor Networks with Empowered Intruders

Haiping Huang, *Member, IEEE*, Tianhe Gong, Rong Zhang, *Senior Member, IEEE*, Lieliang Yang, *Fellow, IEEE*, Jiancong Zhang and Fu Xiao, *Member, IEEE*

***Abstract*—Intrusion detection is one of the important applications of Wireless Sensor Networks (WSNs). Prior research indicated that the barrier coverage method combined with Mobile Sensor Networks (MSNs) can enhance the effectiveness of intrusion detection by mitigating coverage holes commonly appeared in stationary WSNs. However, the trajectories of moving sensors and moving intruders have not been investigated thoroughly, where the impact between two adjacent moving sensors and between a moving sensor and a moving intruder are still undetermined. In order to address these open problems, in this paper, we firstly discuss the virtual potential field between sensors as well as between sensors and intruders. We then propose to formulate the mobility pattern of sensor node using elastic collision model and that of intruder using point charge model. The point charge model describes an hitherto-unexplored mobility pattern of empowered-intruders, which are capable of acting upon the virtual repulsive forces from sensors in order to hide them away from being detected. With the aid of the two models developed, analytical expressions and simulation results demonstrate that our proposed design achieves a higher k-barrier coverage probability in intrusion detection when compared to that of the conventional designs. It is also worth mentioning that these improvements are achieved with shorter average displacement distance and under the much more challenging MSNs settings.**

***Index Terms*—Mobile sensor networks, intrusion detection, k-barrier coverage, empowered intruders**

I. Introduction

1.1 *Motivation*

Intrusion detection can be defined as the technique to detect unapproved entrance into specific territory and it has become the basis of other monitoring applications such as border surveillance and sabotage detection. Traditional radar systems can be utilized in intrusion detection tasks but face the limitations of high cost and high false alarm rates. Moreover, radar systems need to be built in security areas with a long construction cycle. Therefore, distributed target detection systems are proposed in order to address the above problems and provide better performance. Wherein, wireless sensor networks (WSNs) have been widely applied as a kind of low-cost and easy-deployed distributed intrusion detection systems [1] through continuously sensing and transmitting environmental-related data [2], [3]. Multiple sensors may collaboratively judge whether an intrusion event occurs based on decision fusion [4]–[6] and local voting [7]; and multiple sensors also may collaboratively detect the intruder's movement and crossing trajectory by trans-location and coverage optimization, which is exactly the concern of this paper. This issue usually focuses on how to effectively deploy sensor nodes on a specific zone boundary in order to capture an intruder with high probability.

Prior research indicated that the coverage optimization methods, especially the barrier coverage method, are capable of improving the intrusion detection capability in WSNs. Barrier coverage was firstly introduced in [8] for stationary WSNs, where sensors deployed over a belt region are used to carry out intrusion detection and the region is said to provide k-barrier coverage if every path that crosses the width of the belt is covered by at least k distinct fixed sensors ($k \geq 1$). In stationary WSNs, there may exist exposed paths for intruders which cannot be covered by any deployed sensor owing to their 'static' nature. Hence, it is believed that Mobile Sensors Networks (MSNs), where every sensor can move to an appropriate position according to coverage requirements, are capable of enhancing coverage and of avoiding exposed paths appeared in stationary WSNs. However, if the trajectories of moving sensors and moving intruders were completely stochastic, it would be very challenging to justify whether MSNs still provide k-barrier coverage. As a result, it becomes highly desirable to develop a rigorous model for characterizing the k-barrier coverage probability of MSNs.

In this context, virtual potential field based modeling between moving sensors and moving intruders appears to be attractive. This model was firstly adopted in [9], where the field is constructed in such a way that each sensor is repelled by both obstacles and other sensors, thereby forcing the network to spread itself throughout the environment. However, the existing studies of [10], [11] only considered general

This work of H.-P. Huang, T.-H. Gong and F. Xiao was supported by the National Natural Science Foundation of China under Grant 61672297, by the Jiangsu Natural Science Foundation for Excellent Young Scholar under Grant BK20170039 & BK20160089, by the Key Research and Development Program of Jiangsu Province (Social Development Program) under Grant BE2017742, and by the Sixth Talent Peaks Project of Jiangsu Province in China under Grant DZXX-017. The work of R. Zhang and L.-L. Yang was supported by the Engineering and Physical Sciences Research Council, U.K.

H.-P. Huang, T.-H. Gong and F. Xiao are with the School of Computer Science and Technology, Jiangsu High-technology Research Key Laboratory for Wireless Sensor Networks, Broadband Wireless Communication and Sensor Network Technology Key Lab of Ministry of Education, Nanjing University of Posts and Telecommunications, Nanjing 210003, China (E-mail: hhp@njupt.edu.cn; g405252865@163.com; xiaof@njupt.edu.cn).

R. Zhang and L.-L. Yang are with the School of Electronics and Computer Science, University of Southampton, SO17 1BJ, UK. (E-mail: rz,lly@ecs.soton.ac.uk).

J.-C. Zhang is with the Department of Computer Science, University of Bristol, Bristol, U.K. (E-mail: jiancong.zhang@outlook.com).

MSNs setting, where the intruder's crossing trajectories were not taken into account comprehensively. Furthermore, some intruders who are probably equipped with sensing magnetic field scanner may strategically hide them away from sensors. And these intruders are called as empowered intruders who achieve the dodging when acting upon the virtual repulsive forces between sensors and them. Little existing research considers such scenario with the empowered intruders, and meanwhile the barrier coverage probability obtained from current approaches may be further improved. This motivates us to study this hitherto-unexplored problem with novel system models and powerful intrusion detection strategies, where both of them will be treated in this paper.

1.2 *Related work*

Intrusion detection was first introduced in sensor-based robotic systems [12]. It has been an important branch of the coverage problem, which can be divided into two categories: full coverage and barrier coverage. Full coverage needs to ensure the connectivity and maximize the detection rate of the coverage area, while barrier coverage needs to minimize the probability of undetected enemy penetration through the barrier.

The problem of full coverage has been extensively studied in [9], [13] and [14], among which the approach based on virtual potential field [9] attracts considerable attention. [13] and [14] respectively consider the enhanced virtual potential field algorithm and the optimal mobile sensor redeployment strategy, for the purpose of the minimum nodes and the maximal coverage. H. Mahboubi et al. combine the Voronoi diagram with virtual force algorithm and propose a distributed approach of coverage optimization [15]. F. J. Parrado-Garcia et al. study the WSNs deployment configuration for in-situ lunar surveys in which simulated annealing algorithm is used to solve a constrained coverage optimization problem in this application scenario [16]. However, it is difficult for full coverage to thoroughly address the intrusion detection problem due to lack of considerations of moving trajectories of sensors or intruders, and subsequently plenty of research contents have begun to explore barrier coverage in WSNs.

Based on distinctive views of barrier coverage, many solutions are proposed to adapt to different requirements in stationary WSNs. B. Liu et al. present an efficient distributed algorithm to construct sensor barriers on long strip areas of irregular shape without any constraint on crossing paths [17]. A. Chen et al. design a set of metrics in order to measure the quality and performance of barrier coverage in [18]. Taking the moving trajectory, speed and location of moving target (i.e. moving intruder) into account, [19], [20] and [21] respectively provide the effective proposal, where S. Kumar et al. consider the movements of intruder are likely to follow a shorter path when the intruder crosses a belt region [19], and J. M. Chen et al. restrict the farthest distance that an intruder can move without being detected [21], both of which motivating the pattern of intruder's pass-through in this paper. The existence of the exposed path in stationary WSNs hinders it from being the ideal solution in critical intrusion detection tasks where any unmonitored crossing is intolerable.

Currently, mobile WSNs have gradually become the concern of barrier coverage, which are investigated in [10], [11] and [22]–[29]. Where [23]–[25] and [11] illustrate that node mobility may improve the coverage performance of WSNs.

H. Xu et al. design a barrier coverage method in a hybrid sensor networks where the mobile sensors with adjustable sensing ranges can efficiently mend the barrier gaps produced by the stationary nodes [22]. S. J. Li et al. suggest a barrier coverage method which minimizes the maximum sensor movement distance by characterizing critical permutation switches [23]. M. Rout et al. propose two distributed deployment schemes where mobile sensor nodes are randomly deployed over a rectangular belt to form sensor barriers by self-adjustment [24]. Particularly for the scenario of sparse WSNs, S. B. He et al. design a periodic monitoring scheduling (PMS) algorithm in which each point along the barrier line is monitored periodically by mobile sensors to guarantee the high coverage [25]. D. Van et al. extend the traditional virtual force algorithm with interest-driven virtual force to provide monitoring of a moving phenomena in an unknown and open area [28]. G. Y. Keung et al. introduce the gas kinetic theory and mean free path from physics to facilitate the study regarding the intrusion detection problem [11]. Based on these physics models, it derives the inherent relationship between the k-barrier coverage performance and a set of crucial dynamic aspects of MSNs and calculates the detection probability for at least k number of sensor coverage [11]. Nevertheless, the movement pattern of sensor nodes in [11] is purely stochastic so that their sensing area may overlap, which results in a decreased overall detection probability.

Furthermore, literature [10], [26] and [27] focus on developing algorithms to reposition mobile sensors. C. Shen et al. formulate the problem of minimum-energy barrier-coverage, and realize the energy-efficient sensor relocation by utilizing fewer mobile sensors than stationary sensors to achieve barrier coverage [10]. N. Bartolini et al. focus on the vulnerabilities of the deployment based on Voronoi diagrams and put forward a solution to coordinate mobile sensors and guide their movements to new positions [26]. Z. B. Wang et al. mainly study how to efficiently use the reposition of mobile sensors to achieve k-barrier coverage in directional sensor networks [27]. B. Xu et al. investigates the potential of using mobile sensor nodes to strengthen the barrier coverage of WSN by adopting the first-order grey model to determine the vulnerable part of the barrier and relocate mobile nodes to cover the possible loopholes [29]. Particularly, for the bistatic radar (BR) sensor networks, [30] and [31] respectively consider the placement and deployment problem in order to maximize the coverage and minimize the vulnerability of a barrier. However, current deployment strategies of MSNs do not take empowered intruders into consideration and the obtained barrier coverage probability needs to be further improved by designing an effective mobility model of sensor.

To the best of our knowledge, we are the first to study the k-barrier coverage probability in intrusion detection scenario with empowered intruders in MSNs. Based on the virtual potential field, by leveraging the elastic collision model and the point charge model from physics, we investigate the

dynamic relationships between moving intruders and mobile sensors and then evaluate the k-barrier coverage performance in intrusion detection tasks with empowered intruders.

1.3 *Novelty*

In the above-mentioned challenging MSNs setting with empowered intruders, moving sensors are assumed randomly deployed over a belt region, where the movement of each sensor is affected by the virtual repulsive forces between itself and the others. The virtual repulsive forces are considered in this paper because it naturally reduces the overlapping coverage areas between two sensors in order to avoid coverage holes if they are close to each other or causing a collision. We found that the sensor mobility pattern is reminiscent of the $elastic\ collision\ model$. As for empowered intruders, from the view of physical phenomenon, their objective is to cross the parallel boundary of the belt region, with the strategy of acting upon the virtual repulsive forces from moving sensors in order to keep them away from being detected. It turns out that the intruder mobility pattern is very similar to the $point\ charge\ model$. Hence, with the aid of the above two models, we will be able to establish the inherently dynamic relationships between moving sensors and intruders.

Against the above background, the contributions of this paper can be summarized as follows:

• We propose the elastic collision model and the point charge model to describe the mobility patterns of sensors and intruders, respectively. These two models are used for characterizing the k-barrier coverage probability of the challenging MSNs setting, when considering moving trajectories of sensors and empowered intruders.

• With model developments, we further describe the reposition strategies and the dynamic procedure including the collisions among moving sensors and reactions between sensors and empowered intruders. Based on theoretical analysis, experimental results demonstrate that, even under a challenging MSNs setting, our proposal for intrusion detection is capable of achieving a desirable k-barrier coverage probability with less number of sensors when compared to conventional solutions.

1.4 *Organization*

The rest of this paper is organized as follows. Section II describes the problem formulation, mobility model, intrusion detection strategy and gives further discussions on intruders' path-crossing. Simulation results are presented in Section III, and meanwhile further discussion about significance of intruder mobility model is put in this section. Section IV concludes this paper. In addition, the list of primary math symbols can be seen in Tab. I.

II. System Description

2.1 *Problem Formulation*

Consider a MSN consisting of several moving sensors deployed in a rectangular belt region Z as shown in Fig. 1.

TABLE I: DESCRIPTION OF MAIN NOTATIONS

Notation	Description
R	The sensing radius of sensor nodes
k	The multiplicity of barrier coverage requirement
N_Z	The total number of sensor nodes
N_G	The total number of grids
W, H	Width and Height of region Z
S_i	The i-th sensor node
d_{ij}	The distance between S_i and S_j
$\bar{\tau}$	The average time for the intruder to cross a grid
p_i	The probability of one sensor existing in grid i in time interval of τ
N_X	The total number of grids an intruder crosses along with its path
k_v	The virtual force constant
$\vec{v}_i$	The velocity of sensor S_i
$\vec{v}_{ij}$	The relative velocity of sensor S_i with respect to sensor S_j
β	The angle between $\vec{v}_{ij_0}$ and $\vec{n}$
$\mathcal{U}$	The union of neighboring sensors simultaneously colliding with S_j
U	The union of neighboring sensors of one given sensor
R_I	The radius of the intruder's circular track in the point charge model
ρ	The central angle of the circular arc of the intruder's trajectory in the point charge model
θ	Half the central angle corresponding to the intruder's trajectory in the straight crossing model
v_{j_0}	The initial speed of sensor S_j
v_{i_0}	The initial speed of the intruder

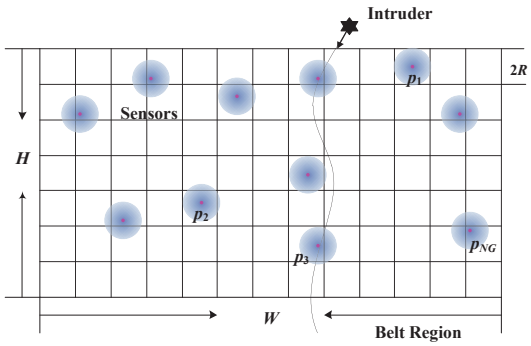

Fig. 1: Intrusion detection problem considered in a MSN.

Initially, these moving sensors are independently deployed with uniform distribution.

The aim of an intruder is to travel across the parallel boundary of region Z, as shown in Fig. 1. We define an intruder which is capable of detecting and escaping from nearby sensors as empowered intruder. The detail analysis of the movement pattern of the empowered intruder can be seen in Point Charge Model in Section 2.2. The intrusion is said to be detected, if the intruder falls within the sensing region of the moving sensors. As a result, a MSN is considered to be k-barrier covered if an intruder is cumulatively detected by at least k moving sensors along its crossing path.

To formulate the probability of k-barrier coverage (denoted by $P(\Lambda \geq k)$), the belt region is divided into quantities of grids as shown in Fig. 1 and the following assumptions should be made:

1. The grid is a square with side length of $2R$ (R is the sensing radius of node). At some point, only one sensor can appear inside one specific grid according to the criterion whether the centroid of this sensor occurs in this grid.

2. $R \ll W$ and $R \ll H$, which indicates that the size of the belt region should be considerably large compared to that of the grid.

3. For mathematical tractability, we adopt the disc-based sensing model, meaning that a sensor can detect an intruder

with probability 1 when the intruder is inside its sensing range and with zero probability of false alarm.

4. The velocity of the intruder is usually considered to be greater than that of the sensor node, otherwise the intruder will be caught easily with high probability. The time it takes for the intruder to cross a grid is denoted by τ.

5. An empowered intruder equipped with sensing magnetic field scanners is able to approximately locate the sensor nodes around itself.

Based on the aforementioned assumptions, we now consider the probability of k-barrier coverage.

As mentioned in assumption 4, the velocity of the intruder is greater than that of the sensor node. Therefore, for a certain grid i, there will be either no sensor nodes (negative event) or at most one sensor node (positive event) inside of it during time interval of τ. For grid i, let p_i be the probability of the aforementioned positive event in time interval τ (and $1-p_i$ be the probability of the negative event accordingly). Note that due to the continuous effect of the elastic collision and virtual force, the frequency of nodes appearing in different grids will vary which results in different value distribution of p_i. This indicates the non-homogeneous property of the spatial distribution of sensor nodes.

Assume that the intruder has crossed a total of N_X grids along its path and is detected by exactly j sensor nodes. Namely, among the N_X grids, there are exactly j grids in which there is one sensor node inside (positive event) when the intruder is crossing it. For a certain event case (among all the possible combinations), the IDs of these j grids can be denoted as $\lambda_1, \lambda_2, ..., \lambda_j$, and the rest of the grids are identified as $\mu_1, \mu_2, ..., \mu_{N_X-j}$, the appearance probability of such an event case is then $\prod_{l=1}^{j} p_{\lambda_l} \cdot \prod_{m=1}^{N_X-j}(1-p_{\mu_m})$.

Assume that the intruder is cumulatively detected by exactly j sensor nodes, to formulate the probability of such cumulative detection, we need to sum up all the possible combinations as

$$P(\Lambda = j) = \sum_{i=1}^{C_{N_X}^{j}} \left(\prod_{l=1}^{j} p_{\lambda_l} \cdot \prod_{m=1}^{N_X-j}(1-p_{\mu_m})\right) \tag{1}$$

It can be seen that there are totally $C_{N_X}^{j}$ items in this summation.

Therefore, the probability of the intruder being cumulatively detected by at least k nodes can be derived as

$$\begin{aligned} P(\Lambda \geq k) &= \sum_{j=k}^{N_X} P(\Lambda = j) = 1 - \sum_{j=0}^{k-1} P(\Lambda = j) \\ &= 1 - \sum_{j=0}^{k-1} \left(\sum_{i=1}^{C_{N_X}^{j}} \left(\prod_{l=1}^{j} p_{\lambda_l} \cdot \prod_{m=1}^{N_X-j}(1-p_{\mu_m})\right)\right) \end{aligned} \tag{2}$$

In order to estimate the value of the average time of intruder crossing a grid (denoted as τ) which determines the sampling interval of p_i, we propose a novel mobility model in Section 2.2 and an intrusion detection method in Section 2.3. In addition, the distribution characteristic of p_i will be adequately discussed in Appendix A.

2.2 *Mobility Model*

Let us now introduce the mobility model used for modeling the behaviors of the sensors and the empowered intruders based on the virtual potential field.

1) Virtual Potential Field

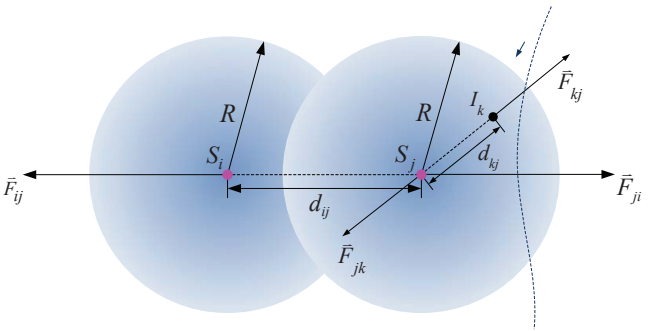

Fig. 2: Illustration of repulsive forces between two sensors or between a sensor and an intruder.

According to the notion of traditional virtual potential field, the virtual repulsive forces usually exist between two adjacent moving sensors. As shown in Fig. 2, considering two sensors S_i and S_j, there exist virtual repulsive forces $\vec{F}_{ij}$ and $\vec{F}_{ji}$ acting on the centroids of the two sensor discs. These forces represent action and reaction to each other with the equal strength and opposite direction. Apart from the virtual repulsive forces between two sensors, we further expand the notion of virtual potential field to include the virtual repulsive forces between a moving sensor and a moving empowered intruder. As shown in Fig. 2, similarly, there exist virtual repulsive forces $\vec{F}_{kj}$ and $\vec{F}_{jk}$ acting on the centroid of a sensor S_j and an intruder I_k, when the intruder enters the S_j's sensing range. In physics, repulsion is inversely proportional to the square of the distance between two entities. Analogously, the virtual repulsive forces can be expressed as

$$\left|\vec{F}_{ij}\right| = \left|\vec{F}_{ji}\right| = k_v d_{ij}^{-2} \text{ or } \left|\vec{F}_{kj}\right| = \left|\vec{F}_{jk}\right| = k_v d_{kj}^{-2} \tag{3}$$

where d_{ij} or d_{kj} is the distance between two sensors or that between a sensor and an intruder, while k_v is the virtual force constant [13]. Under the effect of virtual potential field, motion states of sensors including location and velocity are varying all the time; a collision will occur if two moving sensing discs achieve a adjacently tangent according to the principle of under-mentioned elastic collision model. The instantaneous velocity before elastic collision needs to be calculated, it establishes an important bond between virtual potential field and elastic collision model, and the detailed derivations regarding their relationship can be found in Appendix B.

2) Elastic Collision Model

In principle, the virtual repulsive forces can naturally reduce the overlapping areas covered by two adjacent sensors and collision between their sensing discs, which hence leads to an increased coverage rate. More importantly, this repulsive process is reminiscent of the elastic collision model, which is discussed as follows.

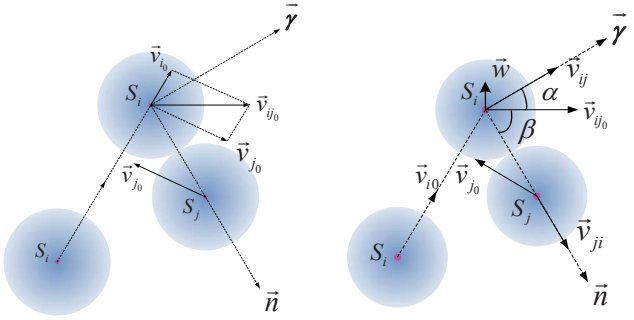

(a) The velocities before single elastic collision occurs

(b) The velocities after single elastic collision occurs

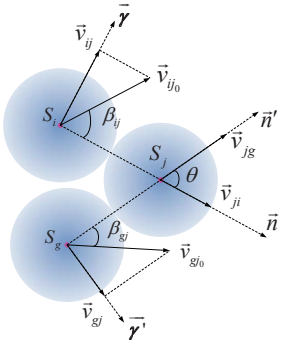

(c) The velocities after multiple elastic collisions occur

Fig. 3: The change of velocities when single or multiple elastic collisions occur.

Let us first consider the single elastic collision model of two moving sensors, S_i and S_j, which, before the collision, have the velocities denoted by $\vec{v}_{i0}$ and $\vec{v}_{j0}$ respectively (the velocity can be solved in Appendix B). Without loss of any generality, let us take sensor S_j as the reference. In this case, $|\vec{v}_{ij0}|=|\vec{v}_{i0}-\vec{v}_{j0}|$ is established, which represents the relative velocity between sensor S_i and sensor S_j before their collision, as shown in Fig. 3(a). Similarly, after the collision, $\vec{v}_{ij}$ (or $\vec{v}_{ji}$) represents the relative velocity of sensor S_i (or S_j) with respect to sensor S_j (or S_i). Furthermore, we adopt the perfect elastic collision model, meaning that the moment of collision is only affected by the virtual repulsive forces between sensors S_i and S_j without any external forces. Then, the interaction between the two sensors obeys the law of conservation of momentum. As a result, with referring to Fig. 3(a), the following system of equations is established (The detailed derivations from (4) to (7) can be referred in Appendix C.)

$$\begin{cases} m_i\,|\vec{v}_{ij}|\sin(\alpha+\beta) = m_i\,|\vec{v}_{ij0}|\sin\beta & (4-1)\\ m_i\,|\vec{v}_{ij}|\cos(\alpha+\beta) + m_j\,|\vec{v}_{ji}| = m_i\,|\vec{v}_{ij0}|\cos\beta & (4-2)\\ m_i\,|\vec{v}_{ij}|\sin\alpha = m_j\,|\vec{v}_{ji}|\sin\beta & (4-3)\\ |\vec{v}_{ij}|\cos(\alpha+\beta) - |\vec{v}_{ji}| = -\,|\vec{v}_{ij0}|\cos\beta & (4-4) \end{cases} \tag{4}$$

where m_i and m_j are the masses of sensors S_i and S_j respectively, while α (or β) is the angle between $\vec{v}_{ij}$ (or $\vec{v}_{ji}$) and $\vec{v}_{ij0}$. After some arrangements of the equations in (4), we can obtain

$$|\vec{v}_{ji}| = 2\cos\beta\cdot|\vec{v}_{ij0}|\cdot m_i/(m_i+m_j) \tag{5}$$

$$|\vec{v}_{ij}| = |\vec{v}_{ij0}|\sqrt{1-4\cos^2\beta\cdot m_i m_j/(m_i+m_j)^2} \tag{6}$$

$$\alpha = \arcsin\left(\sin 2\beta\cdot m_j/\sqrt{(m_i+m_j)^2-4m_i m_j\cdot\cos^2\beta}\right) \tag{7}$$

Note that, when sensors S_i and S_j have the same mass, $|\vec{v}_{ij}|=|\vec{v}_{ij0}|\sin\beta$, $|\vec{v}_{ji}|=|\vec{v}_{ij0}|\cos\beta$ and $\alpha=\pi/2-\beta$ can be readily derived. Hence, after the collision, sensors S_i and S_j exchange their normal velocities, while keeping their tangential velocities constant, as shown in Fig. 3(b). Moreover, the collision is in the direction of the normal vector $\vec{n}$. As seen in Fig. 3(b), the vertical direction of $\vec{n}$ is in the direction determined by the tangential vector of $\vec{\gamma}$.

As shown in Fig. 3(c), when multiple elastic collisions occur between sensor S_j and its neighbors simultaneously, and when assuming that all the sensors have the same mass, the velocity of S_j after the collision can be obtained by summing up all the normal velocities in different directions and be expressed as

$$\vec{v}_j = \sum_{l\in\mathcal{U}}\vec{v}_{jl} + \vec{v}_{j0} \tag{8}$$

where $\vec{v}_{j0}$ is the initial velocity of sensor S_j, $\mathcal{U}$ is the union of the neighbor sensors simultaneously colliding with S_j, and $\vec{v}_{jl}$ is the relative velocity of S_j after the collision with S_l.

3) Point Charge Model

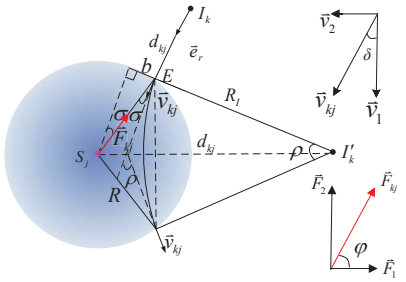

Fig. 4: Illustration of an intruder I_k crossing the sensing region of S_j.

When an intruder enters the sensing region of a sensor, we assume that the intruder's velocity rotates with a constant speed as the result that the virtual repulsive force pushes it away from the sensor. On the other hand, we assume that the sensor's velocity is not affected by the virtual repulsive force between itself and the intruder. Upon considering these effects, we can then model the resultant trajectory of the intruder using the Point Charge Model (PCM) in physics. To elaborate a little further, consider a reference sensor S_j and an intruder I_k. As the virtual repulsive forces between them are internal, the angular momentum of intruder I_k is conservative. We also assume that the intruder's speed is constant, hence its kinetic energy is conservative. Consequently, as shown in Fig. 4, the resultant trajectory of intruder I_k relative to its own position is a circular arc with a radius of R_I, which can be obtained

from the equations of

$$\begin{cases} \left|\vec{F}_{kj}\right| \vec{e}_r = m_k d\vec{v}/dt & (9-1) \\ m_k \cdot d_{kj}^2 \cdot d\sigma/dt = m_k \left|\vec{v}_{kj}\right| b & (9-2) \\ \int d\vec{v} = 2\left|\vec{v}_{kj}\right| \sin(\rho/2) & (9-3) \\ \int \vec{e}_r d\rho = 2\cos(\rho/2) & (9-4) \end{cases} \tag{9}$$

where $\vec{F}_{kj}$ represents the virtual repulsive force between sensor S_j and intruder I_k, $\vec{v}_{kj}$ is the velocity of intruder I_k relative to sensor S_j, and meanwhile $\sin\sigma = b/R$ and $\tan(\rho/2) = R\cos\sigma/(R_I + b)$, as seen in Fig. 4. Furthermore, in (9), $\vec{e}_r$ is the unit direction vector of the repulsive force between sensor S_j and intruder I_k, $\sigma \in (0, \pi/2)$ is the angle between the relative velocity $\vec{v}_{kj}$ and the line connecting S_j and E, as seen in Fig. 4, and finally, ρ is the central angle corresponding to the circular arc of the intruder's trajectory. After some derivations and solutions for the equations in (9), as shown in Appendix D, we obtain

$$\rho = 2\text{arccot}(Rm_k \left|\vec{v}_{kj}\right|^2 \sin\sigma/k_v) \tag{10}$$

Furthermore, the radius R_I of the intruder's circular track can be explicitly expressed as

$$R_I = R\cos\sigma/\tan(\rho/2) - k_v \cot(\rho/2)/(m_k \cdot \left|\vec{v}_{kj}\right|^2) \tag{11}$$

where k_v is a constant of virtual potential field.

2.3 *Intrusion Detection*

1) Average Relative Speed

As shown in Fig. 4, elastic collisions happen when there are virtual repulsive forces existing between sensors and intruders. The limiting case is that two sensing discs are tangent to each other. This happens when the centroids of the neighboring sensors are exactly on the circle with the center of S_j and the radius of $2R$. Given the width and height of the region Z as W and H respectively, as shown in Fig. 1, the average number of neighbor sensors is given by $U = 9\pi R^2 N_Z/(WH) - 1$, where $N_Z/(WH)$ can approximately denote the density of the region. Assume that all sensors have the same mass, after the elastic collisions simultaneously occur between sensor S_j with the initial velocity $\vec{v}_{j0}$ and its U neighbors with the initial velocities $\vec{v}_{1j0}$, $\vec{v}_{2j0}$,$\cdots$, $\vec{v}_{Uj0}$ respectively, the velocity of sensor S_j relative to the lth neighboring sensor is given by $|\vec{v}_{jl}|$=$|\vec{v}_{lj0}|\cos\beta_{jl}$, l=1,2,$\cdots$,U. Consequently, as detailed in Appendix E, the average relative speed between the reference sensor S_j and its U neighbor nodes before the collisions can be obtained from the recursive equations in (67), given as

$$\overline{v}_{1\sim U} = (\overline{v}_{1\sim(U-1)} + |\vec{v}_{jU}|)E_{1\sim U} \tag{12}$$

where $E_{1\sim U}$ is defined in (68).

As the result, the average speed of sensor S_j after the collisions can be figured out as

$$\overline{v}_j = (\overline{v}_{1\sim U} + |\vec{v}_{j0}|)E_j \tag{13}$$

with E_j given by

$$E_j = \frac{2}{\pi}\int_0^{\pi/2} \sqrt{1 - \frac{4\overline{v}_{1\sim U}|\vec{v}_{j0}|\sin^2\varphi}{\overline{v}_{1\sim U}^2 + |\vec{v}_{j0}|^2 + 2\overline{v}_{1\sim U}|\vec{v}_{j0}|}} d\varphi \tag{14}$$

Similarly, after the collision, the average speed of intruder I_k relative to sensor S_j can be derived, which can be expressed as

$$\overline{v}_{kj} = (\overline{v}_k + \overline{v}_j)E_{kj} \tag{15}$$

where $\overline{v}_k$ is the average speed of intruder I_k and

$$E_{kj} = \frac{2}{\pi}\int_0^{\pi/2} \sqrt{1 - 4\overline{v}_k\overline{v}_j/(\overline{v}_k^2 + \overline{v}_j^2 + 2\overline{v}_k\overline{v}_j)\sin^2\varphi} d\varphi. \tag{16}$$

2) Average Cross Time

As shown in Fig. 4, for a given period of time τ, the length of the intruder travels is $\overline{v}_{kj}\tau$. Correspondingly, the intruder has turned $\rho = \overline{v}_{kj}\tau/R_I$ degrees, as seen in Fig. 4, which means the intruder has kept away from the current sensor and the average cross time can be obtained by

$$\begin{aligned} \overline{\tau} &= \frac{R_I\rho}{\overline{v}_{kj}} \\ &= 2\overline{\omega}\cdot(\text{arccot}\overline{\omega})\cdot(\sqrt{R^2m_k^2\overline{v}_{ij}^4 - k_v^2\overline{\omega}^2} - k_v)/(m_k\overline{v}_{kj}^3) \end{aligned} \tag{17}$$

where $\overline{\omega} = (2\pi)^{-1}\int_0^{\pi/2}\omega d\sigma = Rm_k\overline{v}_{kj}^2/(2\pi k_v)$.

During the average cross time τ, whether an intruder is detected by a sensor needs to be judged according to the probability p_i for each grid, which is the precondition of achieving the k-barrier coverage probability. In addition, based on Monte Carlo simulation, the value of N_X can be determined as an intruder crossing through a belt region given a specific experimental scenario.

2.4 *Further Discussions*

In addition to the PCM considered so far, for comparison, in this paper we also consider two mobility models for modeling the intruders' trajectories, which are the Straight Crossing Model (SCM) [11] and the Random Crossing Model (RCM), as demonstrated in Fig. 5(a) and Fig. 5(b), respectively.

Specifically, for the SCM shown in Fig. 5(a), the length of the crossing path is $2R\sin\theta$. Given the average traveling speed $\overline{v}_{kj}$ of an intruder, the time required to cross can be evaluated by (18)

$$\tau = (2R\sin\theta)/\overline{v}_{kj} \tag{18}$$

Furthermore, when considering all the possible crossing paths, the average cross time of the intruder can be expressed as (19)

$$\overline{\tau} = \frac{4R}{\pi\overline{v}_{kj}}\int_0^{\pi/2}\sin\theta dx = \frac{4R}{\pi\overline{v}_{kj}} \tag{19}$$

On the other hand, when assuming the RCM, we may approximate the random trajectory using many short straight crossing paths. As shown in Fig. 5(b), the mobility pattern of the RCM may be described as the intruder conducts a uniform motion for a short period Δt, which is then followed by another uniform motion for the same period Δt with a random

change in moving direction and this continues repeatedly. When the moving duration Δt tends to zero, the intruder's mobility pattern becomes random. Once the intruder gets out of the node sensing disc, all the Δt will be accumulated to achieve the cross time τ. When this process is repeated, we can obtain the average cross time $\overline{\tau}$.

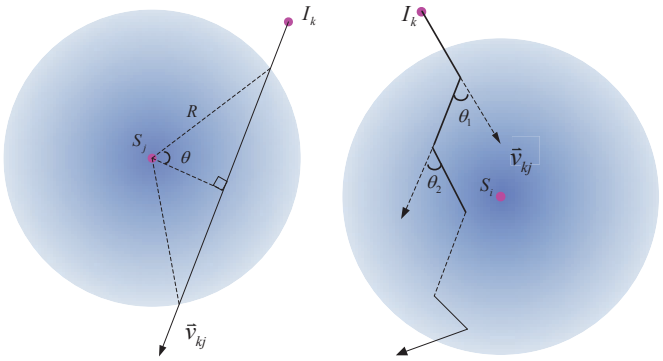

(a) The intruder crosses a sensor's region straightly (b) The intruder crosses a sensor's region randomly

Fig. 5: The intruder crosses a sensor's region by SCM and RCM.

III. Simulation Results

3.1 *Evaluation Methods and Settings*

In this section, we conduct simulations to evaluate the coverage performance of the proposed models and to discuss the dynamic procedure from a new perspective. Unless otherwise specified, the MSN's default simulation settings are shown in Tab. II. For simplicity, the k-barrier coverage of MSNs based on elastic collision and virtual potential field proposed in this paper is called "VMSN" for short, the k-barrier coverage in stationary WSNs is called "WSN" for short, and k-barrier coverage of general MSNs based on gas kinetic theory proposed in [11] is called "gMSN" for short, and the scheme based on classic virtual potential field in [9] and that based on improved virtual potential field in [28] are abbreviated as "CVF" and "VirFID" respectively. The approach based on Grey forecasting model in [29] is abbreviated as "GM". In this paper, "VMSN" is realized by two ways: theoretical evaluation combined with simulations and complete Monte Carlo simulation, denoted as "VMSN(TE)" and "VMSN(MC)", respectively. For the former, equation (1) and (2) are used to calculate the k-barrier coverage probability when p_i, τ and N_X is obtained; while for the latter, actions of both intruders and sensors are completely simulated and the total number of the intruder detected by sensors is recorded in order to achieve the statistical analysis of k-barrier coverage probability. In addition, the k-barrier coverage probability can be figured out in "WSN" and "gMSN". Yet, it is achieved by simulations in "CVF", "VirFID" and "GM". It should be noted that an empowered intruder who obeys point charge model (PCM) is just adopted in "VMSN" and intruders crossing the region randomly (RCM) are used in other schemes. When $N_Z = 100$, R=10m and v_{i0}=30m/s, the comparisons between different schemes regarding the k-barrier coverage probability are shown in Fig. 6.

TABLE II: THE PARAMETERS SETTINGS OF K-BARRIER COVERAGE

Parameter Names	Parameter Values
Size of area	400m (height) × 1200m (width)
Mass of sensor and intruder	1unit
Node number of sensor (N_Z)	100, 200 and 400
Sensing range	R = 10m, 15m or 20m
Sensor's initial speed	10m/s
Intruder's initial speed (v_{i0})	30m/s, 45m/s or 60m/s
The value of k	From 0 to 40
The value of k_v	1, 2

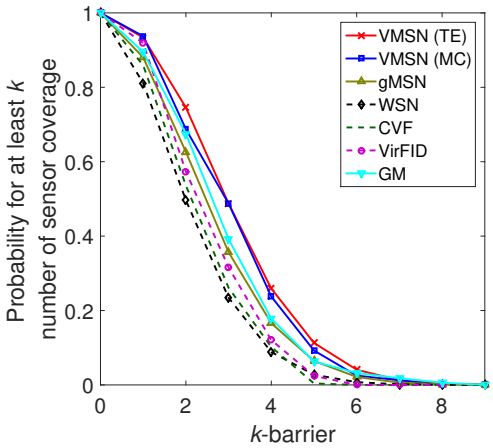

Fig. 6: Probability of k-barrier coverage in different schemes when $N_Z = 100$, R=10m and v_{i0}=30m/s.

From Fig. 6 we can find that the trend of "VMSN(TE)" based on the theoretical evaluation combined with simulations is similar to that of "VMSN(MC)" based on Monte Carlo, and both of them achieve satisfactory performance. The tiny difference between them is originated from limitations of the number of experiments, and the curve of "VMSN(MC)" stays a slightly random fluctuation due to statistical property of simulation results. Actually, due to the influence of estimation of p_i and N_X, even if the curve of "VMSN(TE)" shows more smooth, it is still an approximation of physical truth. Simultaneously, this approximation presents instability which causes that sometimes "VMSN(TE)" is superior to "VMSN(MC)" sometimes on the contrary. In actual, these slight fluctuations of simulation curves are inevitable due to the fact that the number of experiments are not really infinite.

Stationary "WSN" never considers optimizing locations of sensors, so it has a worst performance of detection in most instances. "gMSN" introduces mobile sensor nodes to compensate the coverage holes, yet independent moving tracks may cause overlapping regions, which may decrease the probability of detection. "CVF" employs classic virtual potential field to reduce the overlapping areas among sensors. However, the tending to eventually becoming a static network will weaken the intrusion detection ability of "CVF", and sometimes it shows to be inferior to "WSN" as k value increases. "VirFID" considers the influence of interest event based on virtual potential field, when an intruder is detected by one node, it owns a better interest value, which can attract other nodes to find the intruder. So, its performance is better than "CVF" and even better than "gMSN" in some occasions. However, the network of "VirFID" stays static as well after a period when each node reaches its appropriate position, which will

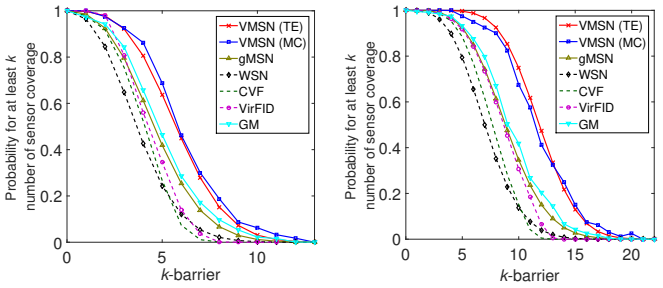

(a) $N_Z = 200$ (b) $N_Z = 400$

Fig. 7: Probability of k-barrier coverage in different schemes when $R = 10$m, $v_{i0} = 30$m/s and N_Z changes.

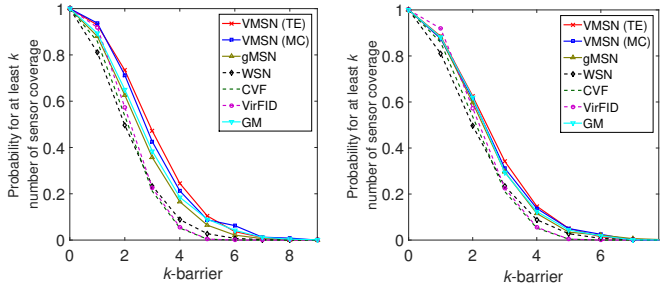

(a) $v_{i0} = 45$m/s (b) $v_{i0} = 60$m/s

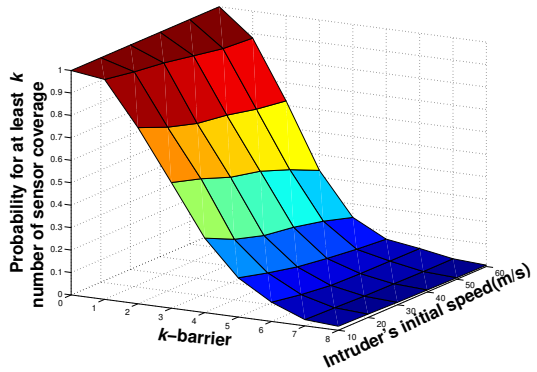

(c) Impact of v_{i0}

Fig. 8: Probability of k-barrier coverage in different schemes when $N_Z = 100$, $R = 10$m and v_{i0} changes.

reduce the probability to catch intruders. Actually, both "CVF" and "VirFID" fail to achieve desirable k-coverage when facing higher k value requirement due to their finally static and relative uniform network characters. And this phenomenon probably results in less sensors gathering in some passing-through paths in "CVF" or "VirFID", which cannot provide a high k-coverage detection. "GM" utilizes the mobility of mobile nodes to cover the loopholes caused by vulnerable static nodes and achieves better k-barrier coverage than "gMSN" when $k \leq 3$. However, the barrier coverage of "GM" with higher k values is not desirable because its design focuses on providing 1-barrier coverage. On the whole, "VMSN" has the best performance because it takes full advantage of virtual potential field and avoids overlapping regions by elastic collisions.

3.2 *Effect of Node Number*

The k-barrier coverage probabilities of "VMSN", "WSN", "gMSN", "CVF", "VirFID" and "GM" with two sets of sensor number (N_Z=200 and 400) are shown in Fig. 7(a) and Fig. 7(b) respectively. It can be seen that the k-barrier coverage probability of "VMSN" are always greater than those of others under the same situations, which benefit from that the sensor mobility can be exploited to compensate for the coverage holes. From Fig. 6, it can be found that the average probability of k-barrier coverage has an increase when N_Z increases, which is consistent with common sense.

3.3 *Effect of Intruder's Initial Speed*

Fig. 8 shows the effect of intruder's initial speed on the k-barrier coverage in different mobility models, where v_{i0} changes into 45m/s in Fig. 8(a) and 60m/s in Fig. 8(b). It can be seen that for each scheme, the faster the intruder moves, the harder the sensors detect him. The change of intruder's initial speed causes more significant effect on "VMSN" and "gMSN" as compared with the other three schemes. Further investigation suggests that when v_{i0} is equal or greater than 60m/s and increases rapidly, the k-barrier coverage probability tends to be mitigatory recession and each scheme provides nearly the same detection level. It can be explained that the time of intruders to cross the region becomes extremely tiny, which makes dynamic mobile network similar to stationary one.

Fig. 8(c) demonstrates the k-barrier coverage of "VMSN" when v_{i0} grows from 10m/s to 60m/s and the inital speed of sensor node is set as 10m/s. It can be seen that the probability of the intruder being k-covered decreases with the increase of v_{i0}, which is consistent with the cases in Fig. 8(a) and Fig. 8(b). In (17), the average cross time is in inverse correlation to the average relative speed $\overline{v}_{kj}$. Greater v_{i0} means greater $\overline{v}_{kj}$ and less average cross time, therefore leads to the decrement in k-coverage probability.

3.4 *Effect of Radius*

Fig. 9 describes the effect of radius on the k-barrier coverage in different mobility models when R changes. As expected, increasing R improves the coverage of sensor nodes and meanwhile raises the chances of intruders being detected. Furthermore, it is shown that "VMSN" provides a better barrier coverage performance than any of others for three values of radius ($R = 10m$ in Fig. 6, $R = 15m$ in Fig. 9(a), $R = 20m$ in 9(b)), which convinces the advantage of "VMSN". From Fig. 9 we can find that when R is above $10m$, the performance of "gMSN" gets worse because the raise of R increases the area of overlap regions. In "CVF", "VirFID" and "VMSN", nodes separate from each other, which causes a higher probability of k-barrier coverage than "gMSN". The barrier coverage of "GM" also improves when R increases. In fact, greater R means it is easier for the mobile sensors to cover the loopholes.

3.5 *Average Displacement Distance*

Furthermore, we also carry out experiments to display the average displacement distance of "VMSN" and "gMSN"

This article has been accepted for publication in a future issue of this journal, but has not been fully edited. Content may change prior to final publication. Citation information: DOI 10.1109/TVT.2018.2872848, IEEE Transactions on Vehicular Technology

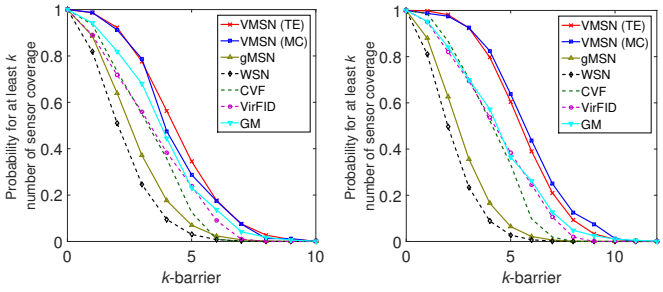

(a) R=15m (b) R=20m

Fig. 9: Probability of k-barrier coverage in different schemes when $N_Z = 100$, v_{i0}=30m/s and R changes.

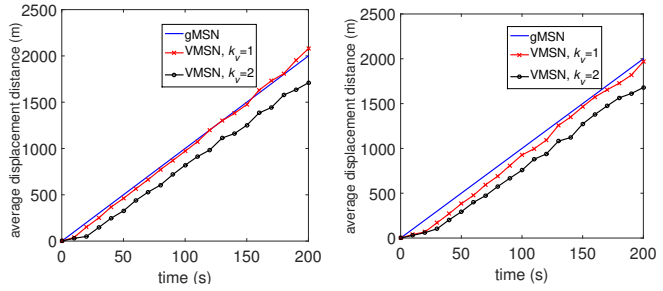

(a) $N_Z = 200$ (b) $N_Z = 400$

Fig. 10: Comparisons of average displacement distance between VMSN and gMSN when N_Z and k_v change.

respectively. We assume an area with 400×1200 size as simulation scene, which tends to be a belt for a practical application involved moving sensor nodes. At the same time, we assume that the whole running time T is partitioned into quantities of unit periods of Δt so that the sensor's motion can be treated as a uniform motion with a straight line approximately within Δt. Every sensor's force, velocity and location are recorded. And the virtual force constant k_v is used to calculate the value of virtual force. We use the same parameters setting as simulation experiments in Fig. 7 in order to effectively measure average displacement distance on the premise that VMSN has better k-barrier coverage performance than gMSN. The average displacement distance of gMSN where sensors move at a constant velocity would not be influenced by the change of parameters due to the moving behaviors of sensors are mutual independent. However, the displacement will probably be varying in VMSN due to the effect of virtual forces and elastic collisions between sensors. Therefore, different k_v and N_Z should be considered in different experimental scenarios to measure the displacement of sensors in VMSN. Fig. 10 (a) shows the comparisons between VMSN and gMSN when $N_Z = 200$, $k_v = 1$ and $k_v = 2$ respectively. Similar comparisons are depicted in Fig. 10 (b) and the distinction from (a) lies in N_Z is set as 400. It can be found that VMSN achieves the minimum average displacement distance when $N_Z = 400$ and $k_v = 2$ through vertical contrasts of (a) and (b) in Fig. 10. Based on observations of experimental process, VMSN can achieve less average displacement distance with the increase of sensor number or virtual force (i.e. k_v).

The increase of sensor nodes in the same belt region will cause the increase of neighbor nodes of any given sensor, which indicates the resultant force from these neighbors will offset each other. Therefore, the average velocities of most sensors especially those located in intermediate region (more neighbors) become slow which results in the decrease in average displacement distance. Furthermore, the virtual force increases between two sensors with the raise of k_v, which means the time spent for sensor deceleration should be extended and the distance traveled in the same time period should become shorter. Simultaneously, in VMSN the average instantaneous velocity after elastic collision trends to a slight decline, this also alleviates the growth of average displacement distance.

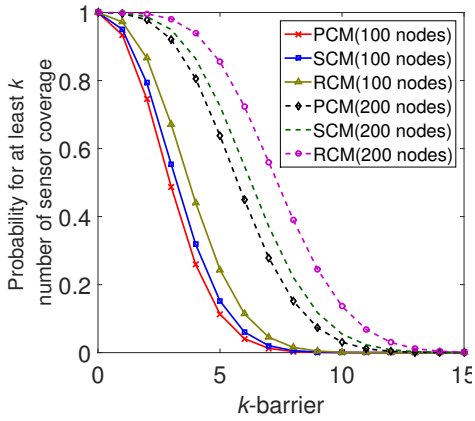

Fig. 11: k-barrier coverage of "PCM", "SCM" and "RCM" in VMSN.

It is noted that some random setting in experimental scenarios such as sensor's initial position and velocity may cause the instability of simulation results because the moving state of sensor is affected by all kinds of resultant forces and elastic collisions from others. And this kind of instability results in fluctuating curve instead of smooth one in VMSN. In addition, not in all cases, VMSN can maintain the advantage of average displacement distance over gMSN. In the same application scenario, appropriate sensor number and virtual constant k_v will enable VMSN to achieve better moving efficiency and k-barrier coverage compared with gMSN.

3.6 *k-barrier coverage among PCM, SCM and RCM*

The point charge model is adopted to describe the trajectory of an empowered intruder who can keep away from being detected by deployed sensors. If models proposed in this paper can still contribute to a high possibility to capture the empowered intruder, it can be convinced that VMSN would obtain more satisfactory performance in general situations with normal intruders.

As mentioned in section 2.4, "SCM" and "RCM" are considered as the models of normal intruder's passing-through instead of empowered intruder's. Fig. 11 shows the average k-coverage performance of "PCM", "RCM" and "SCM" in VMSN ($N_Z = 100$ or $N_Z = 200$) based on virtual potential field, where "SCM" or "RCM" always has a higher possibility to capture a normal intruder than "PCM" to capture an empowered intruder. It is emphasized that both "SCM" and "RCM" models do not take Point Charge Model into account. Furthermore, it can be found that "RCM" achieves better k-barrier coverage performance compared with "SCM" due to

the fact that the intruder in "RCM" may take more time to cross a node's detection region. The average crossing time $\bar{\tau}$ in "RCM" and "SCM" can be shown in Fig. 12 based on amount of experimental analysis and average. As the raise of $\bar{\tau}$, the value of p_i for each grid increases as well, which brings an increase of the detection probability.

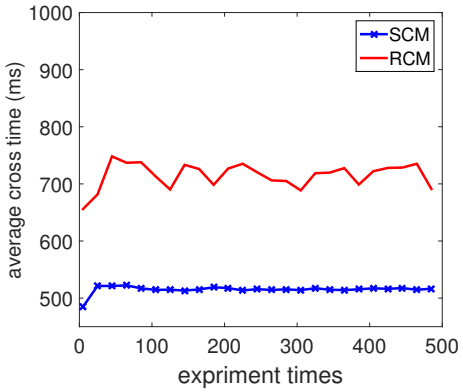

Fig. 12: the value of $\bar{\tau}$ in SCM and RCM.

This is the reason that PCM is just employed in our proposal, which will cause the worse detection performances in other schemes.

IV. Conclusion

In this paper, we have studied the intrusion detection problem of mobile sensor networks with empowered intruders. We firstly discuss the virtual potential field between sensors as well as between sensors and intruders in order to model the trajectories of moving sensors and moving intruders. Elastic collision model and point charge model are respectively employed to formulate the mobility of sensors and that of empowered intruders who are capable of acting upon the virtual repulsive force from sensors in order to keep away from being detected. And then the dynamic relationship between k-barrier coverage probability and the mobility models is established. Simulation experiments combined with theoretical evaluations regarding k-barrier coverage probability are conducted in different schemes, in order to show the more satisfactory coverage performance of VMSN. Furthermore, the average displacement distance is measured between "VMSN" and "gMSN", and the advantage of "PCM" has been verified through the experimental comparisons with "SCM" and "RCM". Consequently, our proposal not only obtains more desirable k-coverage performance but also achieves a guiding significance in future exploration of empowered intruder detection based on MSNs.

In the future, we plan to adopt the probabilistic sensing model to improve the practicability of our current approach. In addition, how to design the moving strategy taken by sensor nodes through tracking and positioning empowered intruders will become the concern of the next research plan in order to further enhance the effectiveness of intrusion detection. In addition, the future work will be implemented in a well-designed testbed to factually verify the intruder detection effectiveness.

Appendix A
Hypothesis Testing Regarding the Distribution of p_i

For one given experimental scenario, p_i for each grid should be measured in order to calculate the k-coverage probability. Meanwhile, we analyze the distribution characters of p_i. At some moment, nodes can only appear in N_Z grids totally while there are no sensors in the remainder grids. The elastic collisions between nodes and region boundaries make nodes to be pushed toward the intermediate region and then spread around due to the collisions with other nodes. Consequently, nodes appearing in the grids which are located at the intermediate region have the higher frequency than nodes appearing in those in the border. Through quantities of simulation experiments of different scenarios, we analyze the statistical property of p_i based on the histogram which obeys normal distribution approximately.

To verify the above guess, hypothesis testing regarding distribution of p_i is necessary aiming at different scenarios. These scenarios involve different scales of regions, different numbers of nodes, different sensing radius, different node motion velocities and different running time in order to reduce the randomness of the experiments. The snapshoot of each grid will be caught to determine whether a sensor arises at a tiny periodic interval (for example, once every τ). After a period of time, the count of node appearing in each grid can be achieved and the histograms regarding the occurrence frequency divided by the total number of experiments can be depicted. Due to the limited space, we cite an example to describe the process of hypothesis testing aiming at one specific scenario. For the convenience of data processing, we observe the statistical frequency of node appearing in each grid (denoted as a random variable x) within the interval τ, and the intensity of frequency is approximate to that of p_i due to the fact that the experiments are numerous and the same for each grid. χ^2 hypothesis testing method is adopted to verify the normal distribution of x with the significance level $\alpha = 0.05$. The hypothesis H_0 is described as follows: the probability density function of x is

$$f(x) = \frac{1}{\sqrt{2\pi}\sigma} e^{-\frac{(x-\mu)^2}{2\sigma^2}}, -\infty \leq x \leq \infty \tag{20}$$

However, the accurate values of parameters μ and σ cannot be obtained, so the moment estimation method should be utilized. We set $\hat{\mu}$ and $\hat{\sigma}$ to represent the estimated values of μ and σ respectively. A data set $\mathbf{D}$ can be used to store the counts of grids with the same frequency for each x (for example, there are total 73 grids with the same frequency of sensor arising i.e. "$x = 25$"), and meanwhile the length of $\mathbf{D}$ (denoted as L_e) can be used to denote the value range of x (in the scenario form 0 to 38). Considering the independent event $A_i = P(x = i)$, and if H_0 is true, the estimated probability density function of x can be represented as

$$\hat{f}(x) = \frac{1}{\sqrt{2\pi}\hat{\sigma}} e^{-\frac{(x-\hat{\mu})^2}{2\hat{\sigma}^2}}, -\infty \leq x \leq \infty \tag{21}$$

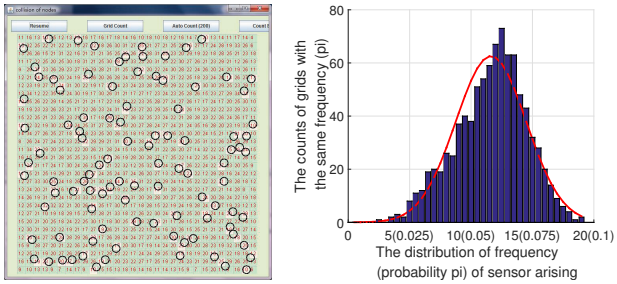

(a) a specific scenario. (b) the distribution characteristics of p_i.

Fig. 13: Hypothesis testing.

and

$$\Sigma = \sum_{i=1}^{L_e} \frac{(N_G f(i) - X_i)^2}{N_G f(i)} \tag{22}$$

where Σ denotes the sum of deviations between the real data and the data from the fitting curve, N_G is the total number of grids, L_e is the length of $\mathbf{D}$, X_i denotes the frequency of sensor arising in one grid. If $\Sigma \leq \chi^2_{0.05}(L_e - r - 1)$ (where r denotes the number of parameters, $r = 2$ in this case: $\hat{\mu} = 23.252$, $\hat{\sigma} = 5.739$), then accept H_0 with the significance level 0.05, i.e. the random variable x obeys the normal distribution.

Fig. 13(b) shows the distribution of x given a specific scenario shown in Fig. 13(a) ($L_1 = 1000m$, $L_2 = 300m$, $N_Z = 80$, $R = 10m$, the total running time is 15 mins, $L_e = 38$, $\mathbf{D} = \{0, 0, 0, 0, 1, 0, 2, 3, 2, 8, 11, 12, 19, 20, 19, 26, 25, 37, 40, 38, 51, 54, 59, 67, 73, 63, 63, 48, 43, 32, 28, 20, 14, 9, 6, 4, 1, 2\}$).

We use matlab tools to examine the hypothesis and distribution property of p_i. Aiming at the case in Fig. 13(a), H_0 is accepted with $\alpha = 0.05$. Lots of simulations with different scenarios are conducted to verify this hypothesis of normal distribution of p_i, and most of them have passed the validation with the satisfactory confidence intervals (or significance level). In Fig. 13(b), it can be found that the data of real distribution is similar to that of the fitting curve of normal distribution with the parameters $\hat{\mu}$ and $\hat{\sigma}$.

APPENDIX B
NODE VELOCITY CALCULATION BASED ON VIRTUAL POTENTIAL FIELD WHEN NODE COLLISION OCCURS

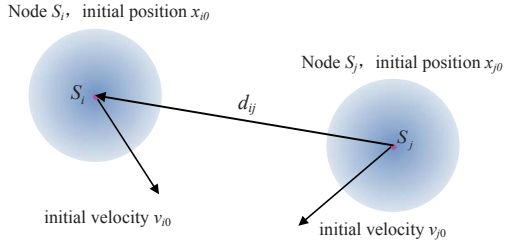

Fig. 14: the initial state of S_i and S_j.

As is shown in Fig. 14, we assume that the initial velocity and position vector of sensor S_i is $\vec{v}_{i0}$ and $\vec{x}_{i0}$, respectively; and that the initial velocity and position vector of sensor S_j is $\vec{v}_{j0}$ and $\vec{x}_{j0}$, respectively; and that the distance vector (from S_j to S_i) between these two sensors is $\vec{d}_{ij}$. Apparently $\vec{d}_{ij}$ is a function of time t and satisfies with $\vec{d}_{ij} = \vec{x}_i - \vec{x}_j$ and $\vec{d}_{ij0} = \vec{x}_{i0} - \vec{x}_{j0}$.

Suppose the quality of S_i and S_j can be denoted as m_i and m_j, respectively. The virtual force the sensor S_i bears can be figured out based on the expression $|\vec{F}_i| = k_v/|\vec{d}_{ij}|^2$. According to Newton's second law, the acceleration of S_i is $\vec{a}_i = \frac{\vec{F}_i}{m_i}$, and its force direction is consistent with that of $\vec{d}_{ij}$, so $\vec{a}_i = \frac{k_v}{m_i|\vec{d}_{ij}|^3}\vec{d}_{ij}$ can be derived. For the sensor node S_i, the expression of its velocity vector can be denoted as $\vec{v}_i = \vec{v}_{i0} + \int_0^t \vec{a}_i \mathrm{d}t$, and that of its position vector can be denoted as $\vec{x}_i = \vec{x}_{i0} + \int_0^t \vec{v}_i \mathrm{d}t$. Finally, we can derive the following expression

$$\vec{x}_i = \vec{x}_{i0} + \int_0^t (\vec{v}_{i0} + \frac{k_v}{m_i}\int_0^t \frac{\vec{d}_{ij}}{|\vec{d}_{ij}|^3}\mathrm{d}t)\mathrm{d}t \tag{23}$$

Similarly, we can derive the expression regarding $\vec{x}_j$ for sensor S_j (its force equals $\vec{F}_i$ but in the opposite direction)

$$\vec{x}_j = \vec{x}_{j0} + \int_0^t (\vec{v}_{j0} - \frac{k_v}{m_j}\int_0^t \frac{\vec{d}_{ij}}{|\vec{d}_{ij}|^3}\mathrm{d}t)\mathrm{d}t \tag{24}$$

In (23) and (24), $\vec{x}_i$, $\vec{x}_j$, $\vec{v}_i$, $\vec{v}_j$ and $\vec{d}_{ij}$ are vector functions of time t.

When $t = 0$, the initial conditions can be represented as follows

$$\begin{cases} \vec{x}_i(0) = \vec{x}_{i0} \\ \vec{x}_j(0) = \vec{x}_{j0} \\ \vec{v}_i(0) = \vec{v}_{i0} \\ \vec{v}_j(0) = \vec{v}_{j0} \end{cases} \tag{25}$$

Subtracting (24) from (23), the final expression regarding $\vec{d}_{ij}$ can be derived

$$\vec{d}_{ij} = (\vec{x}_{i0} - \vec{x}_{j0}) + \int_0^t \left((\vec{v}_{i0} - \vec{v}_{j0}) + 2k_v(m_i^{-1} + m_j^{-1}) \int_0^t \frac{\vec{d}_{ij}}{|\vec{d}_{ij}|^3}\mathrm{d}t \right) \mathrm{d}t \tag{26}$$

The first derivative for (26) can be denoted as

$$\vec{d}'_{ij} = (\vec{v}_{i0} - \vec{v}_{j0}) + 2k_v(m_i^{-1} + m_j^{-1}) \int_0^t \frac{\vec{d}_{ij}}{|\vec{d}_{ij}|^3}\mathrm{d}t \tag{27}$$

And then the second derivative can be denoted as

$$\vec{d}''_{ij} = 2k_v(m_i^{-1} + m_j^{-1}) \frac{\vec{d}_{ij}}{|\vec{d}_{ij}|^3} \tag{28}$$

Decomposing the vector $\vec{d}_{ij}$ along the x and y axis, respectively, we can derive

$$\begin{cases} d''_{ij:x}(t) = 2k_v(m_i^{-1} + m_j^{-1})\left(d_{ij:x}^2(t) + d_{ij:y}^2(t)\right)^{3/2} \cdot d_{ij:x}(t) \\ d''_{ij:y}(t) = 2k_v(m_i^{-1} + m_j^{-1})\left(d_{ij:x}^2(t) + d_{ij:y}^2(t)\right)^{3/2} \cdot d_{ij:y}(t) \end{cases} \tag{29}$$

and further we can achieve the solution of the differential equations in (29) as

$$\begin{cases} d_{ij:x}(t) = f(t, C_1, C_2) \\ d_{ij:y}(t) = g(t, D_1, D_2) \end{cases} \tag{30}$$

where C_1, C_2, D_1 and D_2 are constants.

Take the initial conditions into (30), we can derive

$$\begin{cases} d_{ij:x}(0) = x_{i0:x} - x_{j0:x} \\ d_{ij:y}(0) = x_{i0:y} - x_{j0:y} \\ d'_{ij:x}(0) = v_{i0:x} - v_{j0:x} \\ d'_{ij:y}(0) = v_{i0:y} - v_{j0:y} \end{cases} \tag{31}$$

The values of C_1, C_2, D_1 and D_2 will be solved, among which $x_{i0:x}$ and $x_{i0:y}$ are the respective components of $\vec{x}_{i0}$ on x and y axis; $x_{j0:x}$ and $x_{j0:y}$ are the respective components of $\vec{x}_{j0}$ on x and y axis; the same meaning for $v_{i0:x}$, $v_{i0:y}$ and $v_{j0:x}$, $v_{j0:y}$.

Considering elastic collision occurs between two sensors, we have the following condition

$$\sqrt{d_{ij:x}^2(t) + d_{ij:y}^2(t)} = 2R \tag{32}$$

Substituting the solutions regarding $d_{ij:x}(t)$ and $d_{ij:y}(t)$ into (32), we can achieve the collision time $t = t_c$.

Subsequently the velocity before the coming collision between two sensors can be calculated

$$\begin{cases} \vec{v}_i = \vec{v}_{i0} + \int_0^{t_c} \vec{a}_i \mathrm{d}t \\ \vec{v}_j = \vec{v}_{j0} + \int_0^{t_c} \vec{a}_j \mathrm{d}t \end{cases} \tag{33}$$

So far, we complete the velocity calculation procedure when two sensors collide under the virtual force.

If multiple sensor nodes (p in total) exist, we can observe any one node S_i with its mass m_i, initial velocity vector $\vec{v}_{i0}$ and initial position vector $\vec{x}_{i0}$. Suppose the positions of other nodes are denoted as $\vec{x}_1$, $\vec{x}_2$, $\vec{x}_3$..., $\vec{x}_{p-1}$, according to the principle of electric potential superposition, the acceleration of sensor node S_i can be derived as

$$\vec{a}_i = \sum_{j=1}^{p-1} \frac{k_v m_i^{-1}}{|\vec{x}_i - \vec{x}_j|^3}(\vec{x}_i - \vec{x}_j) \tag{34}$$

And its position at time t can also be calculated

$$\vec{x}_i = \vec{x}_{i0} + \int_0^t \left(\vec{v}_{i0} + k_v m_i^{-1} \int_0^t \sum_{j=1}^{p-1} \frac{\vec{x}_i - \vec{x}_j}{|\vec{x}_i - \vec{x}_j|^3} \mathrm{d}t \right) \mathrm{d}t \tag{35}$$

We can divide time t into so many slots denoted by Δt for the purpose of $\Delta t \to 0$. During Δt, we consider the uniformly accelerated rectilinear motion for each node, so its forward distance approximates to that of uniform rectilinear motion. During the first Δt, the velocity vector and position vector of node S_i can be expressed as (36) and (37), respectively

$$\vec{v}_i = \vec{v}_{i0} + k_v m_i^{-1} \sum_{j=1}^{p-1} \frac{\vec{x}_i - \vec{x}_j}{|\vec{x}_i - \vec{x}_j|^3} \cdot \Delta t \tag{36}$$

$$\vec{x}_i = \vec{x}_{i0} + \vec{v}_i \cdot \Delta t \tag{37}$$

Similarly, the vectors of velocities and positions of other $p-1$ nodes can be calculated and updated by (36) and (37).

APPENDIX C
DERIVATIONS FOR AFTER-COLLISION RELATIVE VELOCITY

As shown in Fig. 3, for the purpose of calculating the after-collision relative velocity of sensor S_i (or S_j) with respect to sensor S_j (S_i), detailed derivations and explanations from (4) to (7) can be described as follows.

Based on the principle of momentum conservation in direction $\vec{\gamma}$, we have

$$m_i \cdot proj(\vec{v}_{ij0}, \vec{\gamma}) = m_i \cdot proj(\vec{v}_{ij}, \vec{\gamma}) \tag{38}$$

where $proj(\vec{x}, \vec{y})$ represents the projection value of vector $\vec{x}$ with respect to vector $\vec{y}$. So (38) can be transformed to (4-1).

Similar to the derivations of (4-1), based on the principle of momentum conservation in direction $\vec{n}$, we have

$$m_i \cdot proj(\vec{v}_{ij}, \vec{n}) + m_j \cdot \vec{v}_{ij} = m_i \cdot proj(\vec{v}_{ij0}, \vec{n}) \tag{39}$$

which can be transformed to (4-2).

In Fig. 3, $\vec{v}_{ij0}$ is the relative velocity between moving sensors S_i and S_j if without any collision. After collision occurs, the resultant momentum of both moving sensors keeps 0 in the direction perpendicularly to $\vec{v}_{ij0}$, and this direction can be denoted as $\vec{w}$. So, we have

$$m_i \cdot proj(\vec{v}_{ij}, \vec{w}) + m_j \cdot proj(\vec{v}_{ji}, \vec{w}) = 0 \tag{40}$$

Considering that the respective projections of $\vec{v}_{ij}$ and $\vec{v}_{ji}$ with respect to $\vec{w}$ have the opposite direction, (40) can be transformed to (4-3).

Due to the characteristics of Perfect Elastic Collision Model, the recovery coefficient (denoted as e) is always 1. Aiming at the direction $\vec{n}$, we have

$$e = \frac{|proj(\vec{v}_{ij}, \vec{n})| - |\vec{v}_{ij}|}{0 - |proj(\vec{v}_{ij0}, \vec{n})|} = 1 \tag{41}$$

Based on (41), (4-4) can be achieved.

From (4-2) and (4-4), we can derive

$$\begin{aligned} m_i\left|\vec{v}_{ij}\right|\cos(\alpha+\beta) &= m_i\left|\vec{v}_{ij0}\right|\cos\beta - m_j\left|\vec{v}_{ji}\right| \\ &= m_i(\left|\vec{v}_{ji}\right| - \left|\vec{v}_{ij0}\right|\cos\beta) \end{aligned} \tag{42}$$

And (42) can be further simplified to

$$\left|\vec{v}_{ji}\right| = 2\frac{m_i}{m_i+m_j}\left|\vec{v}_{ij0}\right|\cos\beta \tag{43}$$

Based on (4-1) and (4-4), we derive (44) and (45) respectively

$$\sin(\alpha+\beta) = \frac{\left|\vec{v}_{ij0}\right|}{\left|\vec{v}_{ji}\right|}\sin\beta \tag{44}$$

$$\cos(\alpha+\beta) = \frac{\left|\vec{v}_{ji}\right| - \left|\vec{v}_{ij0}\right|\cos\beta}{\left|\vec{v}_{ji}\right|} \tag{45}$$

Moreover, based on (44) and (45), we can obtain

$$(\frac{\left|\vec{v}_{ij0}\right|}{\left|\vec{v}_{ji}\right|}\sin\beta)^2 + (\frac{\left|\vec{v}_{ji}\right| - \left|\vec{v}_{ij0}\right|\cos\beta}{\left|\vec{v}_{ji}\right|})^2 = 1 \tag{46}$$

And (46) can be further simplified to

$$\vec{v}_{ij}^2 = \vec{v}_{ji}^2 + \vec{v}_{ij0}^2 - 2\left|\vec{v}_{ji}\right|\left|\vec{v}_{ij0}\right|\cos\beta \tag{47}$$

Based on (43) and (45), we have

$$\begin{aligned} \vec{v}_{ij}^2 &= \vec{v}_{ij0}^2(\frac{4m_i^2\cos^2\beta}{(m_i+m_j)^2} + 1 - \frac{4m_i(m_i+m_j)\cos^2\beta}{(m_i+m_j)^2}) \\ &= v_{ij0}^2(1 - \frac{4m_im_j\cos^2\beta}{(m_i+m_j)^2}) \end{aligned} \tag{48}$$

So

$$\left|\vec{v}_{ij}\right| = \left|\vec{v}_{ij0}\right|\sqrt{1 - \frac{4m_im_j\cos^2\beta}{(m_i+m_j)^2}} \tag{49}$$

Based on (4-3), (43) and (49), we have

$$\sin\alpha = \frac{m_j\left|\vec{v}_{ji}\right|\sin\beta}{m_i\left|\vec{v}_{ij}\right|} = \frac{2m_j\cos\beta\sin\beta}{\sqrt{(m_i+m_j)^2 - 4m_im_j\cos^2\beta}} \tag{50}$$

And (50) can be solved to obtain

$$\alpha = \arcsin\frac{m_j\sin 2\beta}{\sqrt{(m_i+m_j)^2 - 4m_im_j\cos^2\beta}} \tag{51}$$

APPENDIX D
DERIVATIONS FOR CRITICAL PARAMETERS R_I AND ρ

In order to depict the intruder's trajectory accurately, detailed derivations and explanations about critical parameters R_I and ρ can be shown as follows.

Although the direction of force $\vec{e}_r$ from moving sensor S_j to intruder I_k changes at each time point, the value of force $\left|\vec{F}_{kj}\right|$ is kept as a constant. Based on Newton's Second Law of Motion $\vec{F} = m\alpha = m(d\vec{v}/dt)$, we can obtain (9-1).

From Fig. 4, we can calculate the palstance of intruder $\omega_k = \frac{d\sigma}{dt}$, and the initial value of angular momentum for intruder I_k can be described as $\left|\vec{L}\right| = |m(\vec{v}\times\vec{r})|$. So, we have

$$\begin{aligned} \left|\vec{L}_{k(inital)}\right| &= \left|m_k(\vec{v}_{kj}\times\vec{S_j^{\prime}E})\right| \\ &= m_k\left|\vec{v}_{kj}\right|R\sin\sigma = m_k\left|\vec{v_{kj}^{\prime}}\right|b \end{aligned} \tag{52}$$

The value of angular momentum for I_k at any time point can be calculated with $\left|\vec{L}\right| = \left|md^2\omega\right|$. So, we have

$$\left|\vec{L}_k\right| = m_kd_{kj}^2\omega_k = m_kd_{kj}^2\frac{d\sigma}{dt} \tag{53}$$

Since angular momentum is conserved, i.e. $\left|\vec{L}_{k(inital)}\right| = \left|\vec{L}_k\right|$, we can get (9-2).

Just as shown in Fig. 4, the resolution of velocity $\vec{v}_{kj}$ is performed and two sub-velocities $\vec{v}_1$ and $\vec{v}_2$ are generated. The angle between $\vec{v}_{kj}$ and $\vec{v}_1$ is denoted as δ. Because of symmetry, the integral of $\vec{v}_2$ remains 0. During the whole crossing-process of intruder, δ starts from $\rho/2$ to 0 and then back to $\rho/2$. So, we have

$$\begin{aligned} \int d\vec{v} &= \int d\vec{v}_1 = 2\int_0^{\rho/2}\left|\vec{v}_{kj}\right|\cos\delta d\delta = 2\left|\vec{v}_{kj}\right|\sin(\delta)|_0^{\rho/2} \\ &= 2\left|\vec{v}_{kj}\right|\sin(\rho/2) \end{aligned} \tag{54}$$

And (9-3) can be derived from (54).

Similarly, we decompose the virtual repulsive forces $\vec{F}_{kj}$, which now consists of two sub-forces $\vec{F}_1$ and $\vec{F}_2$. The angle between $\vec{F}_{kj}$ and $\vec{F}_1$ is denoted as φ. Because $\sigma+\varphi$ is kept as a constant, we have $d\sigma = -d\varphi$. During the whole crossing-process of intruder, φ starts from $\pi/2-\rho/2$ to 0 and then back to $\pi/2-\rho/2$. And meanwhile, $|\vec{e}_r| = 1$. Hence,

$$\begin{aligned} \int\vec{e}_rd\sigma &= -\int\vec{e}_rd\varphi = 2\int_0^{\pi/2-\rho/2}1\cdot\cos\varphi d\varphi \\ &= (2\sin\varphi)|_0^{\pi/2-\rho/2} = 2\cos(\rho/2) \end{aligned} \tag{55}$$

And (9-4) can be derived from (55).

Based on the geometrical relationship in Fig. 4, we can get $\tan(\rho/2) = R\cos\sigma/(R_I+b)$, i.e.

$$R_I = R\cos\sigma\cot\frac{\rho}{2} - b \tag{56}$$

We multiply (9-1) with (9-2) and get

$$\left|\vec{F}_{kj}\right|\vec{e}_rm_kd_{kj}^2\cdot d\sigma/dt = m_k^2\left|\vec{v}_{kj}\right|b\cdot d\vec{v}/dt \tag{57}$$

Due to $\left|\vec{F}_{kj}\right| = \frac{k_v}{d_{kj}^2}$ (seen in (3)), (57) can be transformed to

$$k_v\vec{e}_rd\sigma = m_k\left|\vec{v}_{kj}\right|b\cdot d\vec{v} \tag{58}$$

Both sides of (58) are performed an integral operation, which is represented by $k_v\int\vec{e}_rd\sigma = m_k\left|\vec{v}_{kj}\right|b\int d\vec{v}$. Based on (3) and (4), $k_v\cdot 2\cos(\rho/2) = m_k\left|\vec{v}_{kj}\right|b\cdot 2\left|\vec{v}_{kj}\right|\sin(\rho/2)$ is established, which can be transformed to (59)

$$m_k\vec{v}_{kj}^2btan(\rho/2) = k_v \tag{59}$$

And the solution regarding b is

$$b = \frac{k_v}{m_k\vec{v}_{kj^2}}\cot(\rho/2) \tag{60}$$

Based on (60), we obtain $\rho = 2\text{arccot}\frac{m_k\vec{v}_{kj}^2b}{k_v}$, and then we substitute $R\sin\sigma$ for b and get

$$\rho = 2\text{arccot}(\frac{m_k\vec{v}_{kj}^2R}{k_v}\sin\sigma) \tag{61}$$

We further put (10) into (56) to eliminate b and achieve (11) (i.e. (62))

$$R_I = R\cos\sigma\cot\frac{\rho}{2} - \frac{k_v}{m_k\vec{v}_{kj}^2}\cot\frac{\rho}{2} \tag{62}$$

APPENDIX E
DERIVATION OF THE AVERAGE RELATIVE SPEED OF MOVING SENSORS

The details of (12) and (13) will be derived as follows.

First, assume two velocities $\vec{x}$ and $\vec{y}$, their lengthes are expressed as $|\vec{x}|$ and $|\vec{y}|$, respectively, while the angle between $\vec{x}$ and $\vec{y}$ is expressed as φ. Then, the relative speed $|\vec{x}-\vec{y}|$ can be expressed as

$$\begin{aligned}|\vec{x}-\vec{y}| &= \sqrt{\vec{x}^2+\vec{y}^2-2|\vec{x}||\vec{y}|\cos\varphi}\\ &= (|\vec{x}|+|\vec{y}|)\sqrt{\frac{\vec{x}^2+\vec{y}^2-2|\vec{x}||\vec{y}|\cos\varphi}{\vec{x}^2+\vec{y}^2+2|\vec{x}||\vec{y}|}}\\ &= (|\vec{x}|+|\vec{y}|)\sqrt{\frac{\vec{x}^2]+\vec{y}^2+2|\vec{x}||\vec{y}|-2|\vec{x}||\vec{y}|(1+\cos\varphi)}{\vec{x}^2+\vec{y}^2+2|\vec{x}||\vec{y}|}}\\ &= (|\vec{x}|+|\vec{y}|)\sqrt{1-\frac{2|\vec{x}||\vec{y}|(1+\cos\varphi)}{\vec{x}^2+\vec{y}^2+2|\vec{x}||\vec{y}|}}\end{aligned} \tag{63}$$

Considering that the angle φ obeys a uniform distribution in $[0\ 2\pi)$, the average relative speed of $|\vec{x}-\vec{y}|$ can be expressed as

$$\begin{aligned}\overline{|\vec{x}-\vec{y}|} &= \frac{1}{2\pi}\int_0^{2\pi}|\vec{x}-\vec{y}|\,d\varphi\\ &= \frac{|\vec{x}|+|\vec{y}|}{2\pi}\int_0^{2\pi}\sqrt{1-\frac{2|\vec{x}||\vec{y}|(1+\cos\varphi)}{\vec{x}^2+\vec{y}^2+2|\vec{x}||\vec{y}|}}d\varphi\\ &= \frac{|\vec{x}|+|\vec{y}|}{\pi}\int_0^{\pi}\sqrt{1-\frac{4|\vec{x}||\vec{y}|(1+\cos\varphi)}{2(\vec{x}^2+\vec{y}^2+2|\vec{x}||\vec{y}|)}}d\varphi\end{aligned} \tag{64}$$

Let $M_{\vec{x},\vec{y}} = \frac{4|\vec{x}||\vec{y}|}{\vec{x}^2+\vec{y}^2+2|\vec{x}||\vec{y}|}$, $\varphi' = 2\varphi$. Then, (64) can be simplified to

$$\begin{aligned}\overline{|\vec{x}-\vec{y}|} =& \frac{2(|\vec{x}|+|\vec{y}|)}{\pi}\int_0^{\pi/2}\sqrt{1-M_{\vec{x},\vec{y}}\sin^2\varphi}d\varphi\\ =&(|\vec{x}|+|\vec{y}|)E_{\vec{x},\vec{y}}\end{aligned} \tag{65}$$

where $E_{\vec{x},\vec{y}}$ is given by

$$\begin{aligned}E_{\vec{x},\vec{y}} &= \frac{2}{\pi}\int_0^{\pi/2}\sqrt{1-M_{\vec{x},\vec{y}}\sin^2\varphi}d\varphi\\ &= \frac{2}{\pi}\int_0^{\pi/2}\sqrt{1-\frac{4|\vec{x}||\vec{y}|}{\vec{x}^2+\vec{y}^2+2|\vec{x}||\vec{y}|}\sin^2\varphi}d\varphi\end{aligned} \tag{66}$$

In order to calculate the average relative speed between the reference sensor S_j and its U neighbor nodes before collisions, (65) is recursively used U-1 times with each time considering two sensors, which can be expressed as

$$\begin{cases}\overline{v}_{1\sim2} = (|\vec{v}_{j1}|+|\vec{v}_{j2}|)E_{1\sim2}\\ \overline{v}_{1\sim3} = (\overline{v}_{1\sim2}+|\vec{v}_{j3}|)E_{1\sim3}\\ \quad\vdots\\ \overline{v}_{1\sim U} = (\overline{v}_{1\sim(U-1)}+|\vec{v}_{jU}|)E_{1\sim U}\end{cases} \tag{67}$$

where the first equation has the same form as (65), while for the others we have

$$\begin{aligned}&E_{1\sim(l+1)}\\ &= \frac{2}{\pi}\int_0^{\pi/2}\sqrt{1-\frac{4\overline{v}_{1\sim l}\left|\vec{v}_{j(l+1)}\right|\sin^2\varphi}{\overline{v}_{1\sim l}^2+\left|\vec{v}_{j(l+1)}\right|^2+2\overline{v}_{1\sim l}\left|\vec{v}_{j(l+1)}\right|}}d\varphi\end{aligned} \tag{68}$$

Finally, the average relative speed between the reference sensor S_j and its U neighbor nodes before collisions is given by $\overline{v}_{1\sim U}$.

REFERENCES

[1] Y. Wang, W. Fu, and D. P. Agrawal, "Gaussian versus uniform distribution for intrusion detection in wireless sensor networks," *IEEE Trans. Parallel Distrib. Syst.*, vol. 24, no. 2, pp. 342–355, Feb. 2013.

[2] H. Yetgin, K. T. K. Cheung, M. El-Hajjar, and L. Hanzo, "Cross-Layer Network Lifetime Maximization in Interference-Limited WSNs, " *IEEE Trans. on Veh. Technol.*, vol. 64, no. 8, pp.3795-3803, Aug. 2015.

[3] R. Kyusakov, J. Eliasson, J. Delsing, J. van Deventer, and J. Gustafsson, "Integration of wireless sensor and actuator nodes with IT infrastructure using service-oriented architecture," *IEEE Trans. on Ind. Informat.*, vol. 9, no. 1, pp. 43-51, Feb. 2013.

[4] D. Ciuonzo and P. Salvo. Rossi, "Distributed detection of a non-cooperative target via generalized locallyoptimum approaches," *Inform. Fusion*, vol. 36, pp. 261–274, Jul. 2017.

[5] D. Ciuonzo, G. Papa, G. Romano, P. Salvo. Rossi, and P. Willett, "One-bit decentralized detection with a rao test for multisensor fusion," *IEEE Signal Process. Lett.*, vol. 20, no. 9, pp. 861–864, Sep. 2013.

[6] D. Ciuonzo, A. De Maio, and P. Salvo. Rossi, "A systematic framework for composite hypothesis testing of independent bernoulli trials," *IEEE Signal Process. Lett.*, vol. 22, no. 9, pp. 1249–1253, Sep. 2015.

[7] N. Katenka, E. Levina, and G. Michailidis, "Local vote decision fusion for target detection in wireless sensor networks," *IEEE Trans. on Signal Process.*, vol. 56, no. 1, pp. 329–338, Jan. 2008.

[8] S. Kumar, T.H. Lai, and A. Arora, "Barrier coverage with wireless sensors," in *Proc. ACM MobiCom*, Aug. 2005, pp. 284-298.

[9] A. Howard, M. J. Matari, and G. S. Sukhatme, "Mobile sensor network deployment using potential field: A distributed scalable solution to the area coverage problem," in *Proc. 6th Int. Symp. on Distributed Autonomous Robotics Systems (DARS02)*, Jun. 2002, pp. 299-308.

[10] C. Shen, W. Cheng, X. Liao, and S. Peng, "Barrier coverage with mobile sensors," in *Proc. IEEE Int. Symp. Parallel Archit., Algor., Netw.*, Jul. 2008, pp. 99-104.

[11] G.Y. Keung, B. Li, and Q. Zhang, "The intrusion detection in mobile sensor network," *IEEE/ACM Trans. on Networking*, vol. 20, no. 4, pp. 1152-1161, Aug. 2012.

[12] D. W. Gage, "Command control for many-robot systems," in *Proc. 19th Annu. AUVS Tech. Symp.*, Jun. 1992, pp. 28-34.

[13] J. J. Huang, L. J. Sun, R. C. Wang, and H. P. Huang, "Improved Virtual Potential Field Algorithm Based on Probability Model in Three-Dimensional Directional Sensor Networks," *Int. J. Distrib. Sens. N.*, Article ID 942080, 9 pages, 2012, Volume 2012, doi:10.1155/2012/942080.

[14] Z. Shen, Y. Chang, H. Jiang, Y. Wang, and Z. Yan, "A Generic Framework for Optimal Mobile Sensor Redeployment," *IEEE Trans. on Veh. Technol.*, vol.59, no.8, pp. 4043-4057, Oct. 2010.

[15] H. Mahboubi and A. G. Aghdam, "Distributed deployment algorithms for coverage improvement in a network of wireless mobile sensors: Relocation by virtual force," *IEEE Transactions on Control of Network Systems*, 2016 online, doi:10.1109/TCNS.2016.2547579.

[16] F. J. Parrado-Garcia, J. Vales-Alonso, and J. Alcaraz, "Optimal planning of wsn deployments for in situ lunar surveys," *IEEE Trans. Aerosp. Electron. Syst.*, 2017 online, doi:10.1109/TAES.2017.2674258.

[17] B. Liu, O. Dousse, J. Wang, and A. Saipulla, "Strong barrier coverage of wireless sensor networks," in *Proc. ACM MobiHoc*, May. 2008, pp.411-420.
[18] A. Chen, T. Lai, and D. Xuan, "Measuring and guaranteeing quality of barrier-coverage in wireless sensor networks," *ACM Trans. on Sensor Networks*, vol.6, no.1, pp.1-31, Dec. 2009.
[19] S. Kumar, T. Lai, M. Posner, and P. Sinha, "Maximizing the lifetime of a barrier of wireless sensors," *IEEE Trans. on Mobile Comput.*, vol.9, no.8, pp.1161-1172, Aug. 2010.
[20] J. K. Li, J. M. Chen, and T. H. Lai, "Energy-efficient intrusion detection with a barrier of probabilistic sensors," in *Proc. IEEE INFOCOM*, Mar. 2012, pp.118-126.
[21] J. M. Chen, J. L. Lai, and T. H. Lai, "Trapping Mobile Targets in Wireless Sensor Networks: An Energy-Efficient Perspective," *IEEE Trans. on Veh. Technol.*, vol.62, no.7, pp.3287-3300, Sep. 2013.
[22] H. Xu, Z. Y. Lai, and C. Liu, "Energy Efficient Movement of Wireless Sensors with Adjustable Sensing Ranges for Mending Barrier Gaps," in *Workshop on Computing, Networking and Communications (CNC), Int. Conf. on Computing, Networking and Communications (ICNC)*, Feb. 2016, pp.1-5.
[23] S. J. Li, and H. Shen, "Minimizing the Maximum Sensor Movement for Barrier Coverage in the Plane," in *Proc. IEEE INFOCOM*, Apr. 26-May. 1 2015, pp.244-252.
[24] M. Rout, and R. Roy. "Self-Deployment of Randomly Scattered Mobile Sensors to Achieve Barrier Coverage." *IEEE Sens. J.*, vol.16, no.18, pp. 6819-6820, Sep. 2016.
[25] S. B. He, J. M. Chen, X. Li, X. M. (Sherman) Shen, and Y. X. Sun, "Mobility and Intruder Prior Information Improving the Barrier Coverage of Sparse Sensor Networks," *IEEE Trans. on Mobile Comput.*, vol. 13, no. 6, pp.1268-1282, Jun. 2014.
[26] N. Bartolini, S. Ciavarella, S. Silvestri, and T. L. Porta. "On the vulnerabilities of Voronoi-based approaches to mobile sensor deployment." *IEEE Trans. on Mobile Comput.*, vol.15, no.12, pp. 3114-3128, Dec. 2016.
[27] Z. B. Wang, J. L. Liao, Q. Cao, H. R. Qi, and Z. Wang, "Achieving k-Barrier Coverage in Hybrid Directional Sensor Networks," *IEEE Trans. on Mobile Comput.*, vol. 13, no. 7, pp.1443-1455, Jul. 2014.
[28] D. Van Le, H. Oh, and S. Yoon, "Virfid: A virtual force (vf)-based interest-driven moving phenomenon monitoring scheme using multiple mobile sensor nodes." *Ad Hoc Netw.*, vol. 27, pp. 112–132, Apr. 2015.
[29] B. Xu, Y. Zhu, D. Kim , D. Li, H. Jiang and A. O. Tokuta, "Strengthening barrier-coverage of static sensor network with mobile sensor nodes." *Wireless Netw.*, vol. 22, no. 1, pp.1-10, Jan. 2016.
[30] X. W. Gong, J. S. Zhang, D. Cochran, and K. Xing."Optimal placement for barrier coverage in bistatic radar sensor networks." *IEEE/ACM Trans. on Networking*, vol. 24, no.1, pp.259-271, Jan. 2016.
[31] B. Wang, J. Y. Chen, W. Y. Liu, and L. T. Yang, "Minimum Cost Placement of Bistatic Radar Sensors for Belt Barrier Coverage," *IEEE Trans. on Comput.*, vol. 65, no. 2, pp. 577-588, Feb. 2016.

Haiping Huang (M'07) received the B.Eng. degree and M.Eng. degree in Computer Science and Technology from Nanjing University of Posts and Telecommunications, Nanjing, China, in 2002 and 2005, respectively; and the Ph.D. degree in Computer Application Technology from Soochow University, Suzhou, China, in 2009. From May 2013 to November 2013, he was a Visiting Scholar with the School of Electronics and Computer Science, University of Southampton, Southampton, U.K. He is currently a professor with the School of Computer Science and Technology, Nanjing University of Posts and Telecommunications, Nanjing, China. His research interests include information security and privacy protection of wireless sensor networks.

Tianhe Gong received the B.Eng. degree in Information Security from Nanjing University of Posts and Telecommunications, Nanjing, China, in 2014. He is currently with successive postgraduate and doctoral programs of study with the School of Computer Science and Technology, Nanjing University of Posts and Telecommunications, Nanjing, China. His research interests include information security and privacy protection of wireless sensor networks.

Rong Zhang (M'09-SM'15) received the B.Sc. degree from Southeast University, China, in 2003, and the Ph.D. degree from Southampton University, U.K., in 2009. He was an Engineer with China Telecom from 2003 to 2004 and also a Research Assistant with the Mobile Virtual Center of Excellence (MVCE), U.K., from 2006 to 2009. He was a Post-Doctoral Researcher with Southampton University from 2009 to 2012. He took an industrial consulting leave from 2012 to 2013 for Huawei Sweden R&D as a System Algorithms Specialist. Now he is an assistant professor at Southampton University. He has authored over 40+ journals in prestigious publication avenues (e.g., the IEEE and OSA) and many more in major conference proceedings. He serves as a Reviewer of the IEEE TRANSACTIONS/JOURNALS and has served several times as a TPC Member/Invited Session Chair of major conferences. He is a recipient of joint funding from MVCE and EPSRC and is also a Visiting Researcher under the Worldwide University Network.

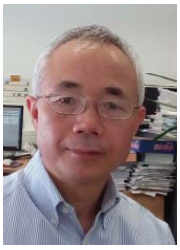

LieLiang Yang (M'98-SM'02-F'15) received the B.Eng. degree in communications engineering from Shanghai Tiedao University, Shanghai, China, in 1988, and the M.Eng. and Ph.D. degrees in communications and electronics from Beijing Jiaotong University, Beijing, China, in 1991 and 1997, respectively. From 1997 to 1997, he was a Visiting Scientist with the Institute of Radio Engineering and Electronics, Academy of Sciences of the Czech Republic. Since 1997, he has been with the University of Southampton, U.K., where he is a Professor of Wireless Communications with the School of Electronics and Computer Science. His research has covered a wide range of topics in wireless communications, networking, and signal processing. He has authored over 290 research papers in journals and conference proceedings. He is a fellow of the IEEE and the IET, served as an Associate Editor of the IEEE TRANSACTIONS ON VEHICULAR TECHNOLOGY, and JOURNAL OF COMMUNICATIONS AND NETWORKS, and he is currently an Associate Editor of the IEEE ACCESS and the Security and Communication Networks journal.

Jiancong Zhang is currently a third-year ar B.Sc. Co. Computer Science student at the University of Bristol, Bristol, U.K. He was a IT Support Assistant at the University of Bristol IT Services in 2017. He now serves as the Vice-President of the University of Bristol Chinese Society, being responsible for developing and maintaining the society website. His research interest include information security and web technologies.

Fu Xiao (M'12) received the Ph.D Degree in Computer Science and Technology from Nanjing University of Science and Technology, Nanjing, China, in 2007.
He is currently a Professor and PhD supervisor with the School of Computer Science and Technology, Nanjing University of Posts and Telecommunications, Nanjing, China. His main research interest is Wireless Sensor Networks. Dr. Xiao is a member of the IEEE Computer Society and the Association for Computing Machinery.